ACTN2 mutations cause "Multiple structured Core Disease" (MsCD)

Xavière Lornage, Norma B Romero, Claire A. Grosgogeat, Eduardo Malfatti, Sandra Donkervoort, Michael Marchetti, Sarah B. Neuhaus, A. Reghan Foley, Clémence Labasse, Raphael Schneider, et al.

HHS Public Access

Author manuscript

Acta Neuropathol. Author manuscript; available in PMC 2020 March 01.

Published in final edited form as:

Acta Neuropathol. 2019 March ; 137(3): 501–519. doi:10.1007/s00401-019-01963-8.

ACTN2 mutations cause "Multiple structured Core Disease" (MsCD)

Xavière Lornage[1,2,3,4,*], **Norma B. Romero**[5,6,7,*], **Claire A. Grosgogeat**[8,£], **Edoardo Malfatti**[6,7,9,£], **Sandra Donkervoort**[10], **Michael M. Marchetti**[8], **Sarah B. Neuhaus**[10], **A. Reghan Foley**[10], **Clémence Labasse**[6,7], **Raphaël Schneider**[1,2,3,4], **Robert Y. Carlier**[11,12], **Katherine R. Chao**[13], **Livija Medne**[14], **Jean-François Deleuze**[15], **David Orlikowski**[16], **Carsten G. Bönnemann**[10], **Vandana A. Gupta**[8], **Michel Fardeau**[5,6,7], **Johann Böhm**[1,2,3,4,$], and **Jocelyn Laporte**[1,2,3,4,$]

[1]Institut de Génétique et de Biologie Moléculaire et Cellulaire (IGBMC), 1, rue Laurent Fries, BP 10142, 67404 Illkirch, France

[2]INSERM U1258, 67404 Illkirch, France

[3]CNRS, UMR7104, 67404 Illkirch, France

[4]Université de Strasbourg, 67404 Illkirch, France

[5]Université Sorbonne, UPMC Univ Paris 06, INSERM UMRS974, CNRS FRE3617, Center for Research in Myology, GH Pitié-Salpêtrière, 47 Boulevard de l'hôpital, 75013 Paris, France

[6]Centre de référence de Pathologie Neuromusculaire Paris-Est, Institut de Myologie, GHU Pitié-Salpêtrière, Assistance Publique-Hôpitaux de Paris, Paris, France

[7]Neuromuscular Morphology Unit, Myology Institute, GHU Pitié-Salpêtrière, Paris, France

[8]Division of Genetics, Brigham and Women's Hospital, Harvard Medical School, Boston, MA 02115, USA

[9]Neurology department, Raymond-Poincaré teaching hospital, centre de référence des maladies neuromusculaires Nord/Est/Ile-de-France, AP-HP, Garches, France

[10]Neuromuscular and Neurogenetic Disorders of Childhood Section, National Institute of Neurological Disorders and Stroke, National Institutes of Health, Bethesda, MD 20892, USA

[11]Department of Radiology, Neurolocomotor Division, Raymond Poincare Hospital, University Hospitals Paris–Ile-de-France West, Public Hospital Network of Paris, Garches, France

[12]Versailles Saint-Quentin-en-Yvelines University, Versailles, France

Correspondence: Jocelyn Laporte, IGBMC, 1 Rue Laurent Fries, 67404 Illkirch, France, jocelyn@igbmc.fr / +33 (0)388653412.

*,£,$These authors contributed equally

Author contributions

NBR, CB, JB, JL conceived and designed the study. XL, CAG, SD, MMM, SN, ARF, CL, KRC, LM, JFD performed the experiments. XL, NBR, EM, SD, SN, ARF, RS, RYC, CB, VAG, MF analyzed the data. XL, NBR, MF, JB, JL wrote the manuscript with input from the other coauthors.

Conflict of interest

None of the authors reports conflicts of interest.

[13]Center for Mendelian Genomics, Program in Medical and Population Genetics, Broad Institute of MIT and Harvard, Boston, MA 02115, USA

[14]Division of Human Genetics, The Children's Hospital of Philadelphia, Philadelphia, PA 19104, USA

[15]National Genotyping Center, Genomics Institute, Office of Atomic Energy and Alternative Energies, Evry, France

[16]CIC 1429, INSERM, AP-HP, Hôpital Raymond Poincaré, 92380, Garches, France

Abstract

The identification of genes implicated in myopathies is essential for diagnosis and for revealing novel therapeutic targets. Here we characterize a novel subclass of congenital myopathy at the morphological, molecular, and functional level. Through exome sequencing, we identified *de novo* *ACTN2* mutations, a missense and a deletion, in two unrelated patients presenting with progressive early-onset muscle weakness and respiratory involvement. Morphological and ultrastructural analyses of muscle biopsies revealed a distinctive pattern with the presence of muscle fibers containing small structured cores and jagged Z-lines. Deeper analysis of the missense mutation revealed mutant alpha-actinin-2 properly localized to the Z-line in differentiating myotubes and its level was not altered in muscle biopsy. Modelling of the disease in zebrafish and mice by exogenous expression of mutated alpha-actinin-2 recapitulated the abnormal muscle function and structure seen in the patients. Motor deficits were noted in zebrafish, and muscle force was impaired in isolated muscles from AAV-transduced mice. In both models, sarcomeric disorganization was evident, while expression of wild-type alpha-actinin-2 did not result in muscle anomalies. The murine muscles injected with mutant *ACTN2* displayed cores and Z-line defects. Dominant *ACTN2* mutations were previously associated with cardiomyopathies, and our data demonstrate that specific mutations in the well-known Z-line regulator alpha-actinin-2 can cause a skeletal muscle disorder.

Keywords

ACTN2; alpha-actinin-2; congenital myopathy; core myopathy; Z-line; nemaline myopathy

Introduction

Congenital myopathies are a group of heterogeneous genetic diseases usually associated with neonatal or early-onset hypotonia and muscle weakness, and are characterized by distinctive alterations on muscle biopsies [13, 33, 40]. Although approximately 30 causative genes are known to date (www.musclegenetable.fr), nearly half of the patients with congenital myopathies do not have a molecular diagnosis despite routine access to next-generation sequencing, suggesting the implication of yet unidentified genes. The identification of novel causative genes is a prerequisite to understand the pathophysiological mechanisms underlying muscle dysfunction, and can suggest new and alternative therapeutic targets.

Congenital myopathies are classified into distinct sub-groups based on characteristic histopathological features on muscle biopsies. Most patients fall into one of the three main groups encompassing centronuclear myopathy with numerous fibers containing internal or centralized nuclei, nemaline myopathy showing protein aggregates or rod inclusions, and core myopathy with fiber areas devoid of oxidative activity [40, 42]. Central core disease (CCD) is characterized by well-delimited cores running along the longitudinal myofiber axis, while multiminicore disease (MmD) typically displays multiple, poorly defined, small cores spanning only a limited zone on the longitudinal axis of the muscle fiber [9, 12, 14].

Here we describe a peculiar form of core myopathy with ultrastructural Z-line alterations caused by mutations in *ACTN2*, encoding alpha-actinin-2 (MIM *102573).

ACTN1, *ACTN2*, *ACTN3*, and *ACTN4* form an evolutionary conserved gene family with different tissue-specific expression pattern [32]. *ACTN3* is expressed in skeletal muscle and *ACTN2* is expressed in both skeletal and cardiac muscle. *ACTN3* deficiency is common in humans and influences athletic performances [35], and dominant mutations in *ACTN2* have been reported to cause dilated or hypertrophic cardiomyopathy (MIM #612158 [6]).

Alpha-actinin-2 is one of the major component of the Z-line. It is active as a dimer, allosterically regulated by phosphoinositides [5, 38], and is essential for the integrity of the contractile apparatus through a multitude of interactions. Notably, it binds and crosslinks actin filaments, and anchors many cytoskeletal and sarcomeric proteins such as myopalladin [1], myotilin [41], muscle LIM protein [31], and the giant proteins titin [11, 26] and nebulin [34]. Moreover, alpha-actinin-2 is believed to make a link between the sarcomere and the membrane through interactions with vinculin [30], integrins [36], and the dystrophin complex [21]. Alpha-actinin-2 is also involved in the regulation of ion channels [8, 28], gene expression [23], and signalling cascades [39, 46], making it a multitasking protein with a central role in skeletal muscle physiology. Indeed, alpha-actinin-2 deficiency in the zebrafish was shown to result in sarcomeric defects, confirming its crucial role for the formation and/or maintenance of sarcomeres [19].

This report describes *ACTN2* mutations as the cause of a congenital myopathy with numerous structured cores and jagged Z-lines as the main and specific histological hallmark, and we evidence our findings by functional investigations in cell and animal models. Exogenous expression of mutant alpha-actinin-2 in mice and zebrafish induced muscle weakness and a histopathology corresponding to the unique structural aberrations characterizing the patient biopsies. The implication of *ACTN2* in a skeletal muscle disease and the peculiar histopathology define an additional class of core myopathy.

Material and methods

DNA sampling

Sample collection was performed with written informed consent from patients P1 and P2 according to the declaration of Helsinki and its later amendments. DNA storage and usage was approved by the institutional review board (DC-2012–1693 and 12-N-0095).

MRI

Whole-body MRI in P1 was performed on a 3T magnet system using the Dixon method to obtain T1 and T2-weighted scans. Images were then post-processed with multiplanar reconstructions and 3D volume rendering. Analysis was performed for a selection of 100 muscles manifesting atrophy and fatty infiltrations as described previously [4]. 3D volume rendering images allowed a global analysis in horizontal position. Lower extremity MRI in P2 was performed on a 3T Siemens Magnetom Verio system using the Dixon method to obtain T1 and STIR-weighted scans.

Exome sequencing and analysis

Library preparation and exome capture were performed with the SureSelect Human All Exon 50Mb Capture Library v5 (Agilent, Santa Clara, USA) for P1 and his healthy family members, and with the Nextera Rapid Capture (Illumina, San Diego, USA) for P2 and her healthy parents, and samples were paired-end sequenced on a HiSeq 2500 (Illumina). Sequence data were aligned to the GRCh37/hg19 reference genome, and variants were filtered considering their frequency in gnomAD (http://gnomad.broadinstitute.org/) and in our in-house database containing 1550 exomes and genomes. The mutations were numbered according to GenBank NM_001103.3 and NP_001094.1 with +1 corresponding to the A of the ATG translation initiation codon. Confirmation of variants and segregation was performed by Sanger sequencing. P1 was heterozygous and P2 homozygous for the common p.(Arg577*) *ACTN3* variation.

Morphological studies

For P1, open deltoid muscle and radialis muscle biopsies were respectively obtained at 9 and 45 years of age. Conventional histological and histochemical techniques on 10 μm cryostat sections encompassed Haematoxylin and Eosin (H&E), Gomori Trichrome (GT), Nicotinamide adenosine dinucleotide–tetrazolium reductase (NADH-TR), Succinate dehydrogenase (SDH), and myosin adenosine triphosphatase (ATPase pH 9.4) reactions. Digital photographs were obtained with a Zeiss AxioCam HRc linked to a Zeiss Axioplan Bright Field Microscope and processed with the Axio Vision 4.4 software (Zeiss, Oberkochen, Germany).

For P2, open muscle biopsy of the quadriceps was obtained at 19 years of age. Digital photographs were obtained with a Zeiss AxioCam MRc5 linked to a Zeiss Imager Bright Field Microscope and processed with the AxioVision software (Zeiss).

Murine tibialis anterior muscles were sampled in isopentane cooled in liquid nitrogen, and transversal or longitudinal cryosections (8 μm) were fixed and stained with H&E, SDH, and GT. Images were acquired with the Hamamatsu NanoZoomer 2HT slide-scanner (Hamamatsu, Hamamatsu city, Japan).

Electron microscopy

The P1 patient biopsies were fixed with glutaraldehyde (2.5 %, pH 7.4), post fixed with osmium tetroxide (2 %), dehydrated, and embedded in resin (EMBed-812, Electron Microscopy Sciences, Hatfield, USA). Ultra-thin sections were stained with uranyl acetate

and lead citrate, and observed using a Philips CM120 electron microscope (Philips, Amsterdam, Netherlands) and photo-documented using a Morada camera (Soft Imaging System, Münster, Germany). EM was not available for P2.

Murine TA muscles were fixed in 4% PFA and 2.5% glutaraldehyde in 0.1 M phosphate buffer (pH 7.2) overnight at 4°C and processed as previously described [7]. Images were recorded on a Philips CM12 electron microscope (Philips).

Three dpf zebrafish larvae were fixed in formaldehyde-glutaraldehyde-picric acid in cacodylate buffer overnight at 4°C, followed by osmication and uranyl acetate staining. Subsequently, embryos were dehydrated in a series of ethanol washes and embedded in TAAB Epon (Marivac Ltd., Halifax, Canada). Sections (95 nm) were cut with a Leica UltraCut microtome (Leica, Wetzlar, Germany), picked up on 100-μm Formvar-coated copper grids, and stained with 0.2% lead citrate. Sections were viewed and imaged with a Philips Tecnai BioTwin Spirit electron microscope (Philips) at the Harvard Medical School Electron Microscopy Core.

Cell culture, transfection, and differentiation

The peGFP-ACTN2 construct was a kind gift from Johannes Hell (Addgene plasmid #52669) [20]. The patient's mutation was introduced by site-directed mutagenesis using the QuikChange II kit (Strategene, San Diego, USA). C2C12 cells were transfected with wild-type and mutant constructs using Lipofectamine 3000 (Thermo Fisher Scientific, Waltham, USA), and fixed after 24 h. For differentiation, cells were plated on a BD Matrigel™ Basement Membrane Matrix (Becton Dickinson, Franklin Lakes, USA) 24 h before transfection, and serum-free differentiation medium was applied on confluent cells. Myotubes were fixed at day 8, and immunolabelling was performed as described below.

Immunolocalization

For immunohistochemistry, transverse muscle sections were frozen in isopentane, and longitudinal sections were fixed at 4°C in 4% PFA for 24 h and incubated overnight in 30% sucrose at 4°C. Myoblasts and myotubes were fixed during 20 minutes in 4% PFA. Permeabilization was performed with PBS-Triton 0.2% and saturation with FCS 10% in PBS. Following primary and secondary antibodies were used: rabbit anti-alpha-actinin-2 (ab68167, Abcam, Cambridge, UK), mouse anti-vinculin (V9131, Sigma, St. Louis, USA), Alexa Fluor 488 or 594 goat anti-mouse or anti-rabbit antibodies (Invitrogen, Carlsbad, USA). Images were taken using a SP5-UV confocal microscope (Leica).

Protein studies

For western blot, total muscle lysates were prepared in a buffer containing 50 mM Tris, 100 mM NaCl, 1 mM EGTA, 0.5% NP-40, 0.5% Triton-X100, 0.1% SDS, 1 mM DTT, 1 mM PMSF, and a mix of protease inhibitor (Complete EDTA-free, Roche, Basel, Switzerland). For human muscles, 50 μg of protein extracts were loaded on a 10% SDS-Page gel. For murine muscles, 5 μg of protein extracts were loaded on 4–15% Mini-PROTEAN®TGX™ precast protein gel (Biorad, Hercules, USA). Following primary and secondary antibodies were used: rabbit anti-alpha-actinin-2 (ab68167, Abcam), rabbit anti-alpha-actinin-3

(ab68204, Abcam), mouse anti-actin (homemade), mouse anti-beta-tubulin (homemade), mouse anti-GAPDH (MAB374, Millipore, Burlington, USA), and horseradish peroxidase (Jackson immunoresearch Europe, Cambridgeshire, UK). Membranes were revealed with the Supersignal west pico kit (ThermoFisher Scientific), and all immunoblots were visualized on an Amersham Imager 600 (GE Healthcare Life Sciences, Chicago, USA).

Domain predictions and 3D protein modeling

Alpha-actinin-2 protein domains were annotated using InterPro [15] and the scheme was designed using IBS (Illustrator for Biological Sequences)[27]. The crystal structure data of human alpha-actinin-2 was obtained from the PDB database (4D1E) [38]. Molecular graphics and analyses were performed with the UCSF Chimera package. Chimera is developed by the Resource for Biocomputing, Visualization, and Informatics at the University of California, San Francisco (supported by NIGMS P41-GM103311) [37]. Structure was edited by adding arginine rotamers from the Dunbrack library [10].

Zebrafish experimentation

Zebrafish (*Danio rerio*) from the wild-type Tuebingen line were bred and maintained according to standard procedures [45]. Embryos were collected by natural spawning, staged by hours (hpf) or days (dpf) post fertilization [24], and raised at 28.5°C in egg water. All animal work was performed with approval from the Institute animal care and user committee.

For mRNA overexpression, full-length human *ACTN2* cDNA optimized for expression in zebrafish was synthesized by Eurofins and cloned into a pCSDest destination vector (created by Nathan Lawson) using Gateway technology (Invitrogen). Mutagenesis to incorporate the substitution was performed using the GENEART kit (Invitrogen). Wild-type and mutant mRNA was synthesized *in vitro* using mMessage mMachine SP6 kit (Ambion, Austin, USA).We titrated the mRNA (50–250 ng) and injected 100–200 pg into embryos at the 1-cell stage, and subsequent phenotypic analyses were performed at 3 dpf.

For western blot, zebrafish larvae were homogenized in buffer containing Tris-Cl (20 mM, pH 7.6), NaCl (50 mM), EDTA (1 mM), Nonidet P-40 (0.1%) with complete protease inhibitor cocktail (Roche Applied Sciences, Indianapolis, USA). Primary antibodies were rabbit anti alpha-actinin-2 (4B3, Sigma) and mouse anti-β-actin (A5441, Sigma) [2].Protein bands were quantified using Quantity One software (Biorad).Zebrafish swimming behavior was quantified using the Daniovision activity monitoring system (Noldus, Leesburg, USA). Single mRNA-injected larvae or uninjected controls were placed into 24-well plates. After a 10 minutes acclimation to the dark, larvae were stimulated by light exposure for 20 minutes. Swimming behavior was recorded over the entire 20 minutes period with an infrared light source and total distance travelled was quantified. Three independent trials were performed with larvae from different clutches, examining >300 larvae within each group.

Whole-mount phalloidin staining for filamentous actin was performed on 3 dpf zebrafish larvae as described previously [3]. Briefly, larvae were fixed overnight in 4% PFA at 4°C, then washed 2×10 min in PBS, 2×10 min in PBS-T (0.1% Tween-20), 1× 60 min in PBS-TR (2% Triton X), and 2×5 min in PBS-T. Larvae were blocked in PBS-T containing 5% goat

serum for 1h at RT, and incubated with Alexa Fluor 488 phalloidin (A12379, Invitrogen) overnight at 4°C. Larvae were washed 4×15 min in PBS-T before being mounted in 70% glycerol and visualized using a UltraVIEW VoX spinning disk confocal microscope (Perkin Elmer, Waltham, USA).

Mouse experimentation

C57B6/J mice were purchased at 3 weeks of age from Charles River (L'Arbresle, France), and housed in a temperature-controlled room and in ventilated cages. Experiments were conducted on males according to the French and European legislation on animal care and experimentation.

ACTN2 cDNA was cloned into the plasmid pAAV-MCS (Stratagene, La Jolla, USA) containing the CMV immediate early enhancer and promoter, the human growth hormone poly-adenylation signal and the AAV serotype 2 inverted terminal repeats (ITRs). An empty vector without *ACTN2* cDNA was used as control. pAAV expressing plasmids were co-transfected with pHelper (Stratagene) and pAAV2/9 packaging plasmid (PENN vector core) into a HEK293T-derived cell line using Polyethylenimine transfection reagent. AAV serotype 9 vectors were harvested 48 h after transfection from cell lysate treated with 100U/mL Benzonase (Merck, Darmstadt, Germany). They were purified by iodixanol gradient ultracentrifugation, dialyzed and concentrated using AMICON Ultra-15 100K in DPBS supplemented with 0,5mM MgCl2. Viral titers were determined by Q-PCR using the LightCycler480 SYBR Green I Master (Roche).

AAV injections were performed in 15 male C56B6/J mice. They were anesthetized by intraperitoneal injection of ketamine (20mg/mL), and tibialis anterior muscles were injected with 20 µL wild-type, mutant, or control AAV2/9 (5X10^12 VG/mL). Mice were analyzed 4 weeks post injection as it was shown to be an adequate timing for AAV expression and appearance of morphological defects in skeletal muscle [7].

For in situ muscle force measurements, mice were anesthetized intraperitoneally with pentobarbital (50mg/kg), and the distal tibialis anterior tendon was attached to the force transducer (Aurora Scientific, Aurora, Canada). The absolute maximal force was measured after tetanic stimulation of the sciatic nerve with a pulse frequency from 25 to 125 Hz. The specific maximal force was calculated by dividing the maximal force through the tibialis anterior muscle weight.

Results

Clinical description

P1 is the third child born to healthy non-consanguineous parents. First concerns arose during the neonatal period with moderate hypotonia and sucking difficulties. Cardiomegaly and heart failure were diagnosed at the age of two months, and disappeared by the age of 6 months following treatment with corticosteroids and digitalins. Subsequent cardiac follow-up was normal. The patient achieved independent ambulation from 20 months of age. He was examined at 9 years of age by one of us (MF) and followed for 38 years at the Myology Institute (Paris). At 9 years of age, the patient presented with diffuse muscle atrophy and

extraocular muscle weakness. He underwent Achilles tendons release surgery at age 14 years, and a dorsal kyphoscoliosis was surgically corrected at 16 years of age. The patient lost ambulation at the age of 17 years. At the age of 35 years, respiratory insufficiency with a vital capacity reduced to 37% required night ventilation, which was later replaced by a tracheostomy. The last clinical examination at the age of 45 years revealed generalized atrophy, bilateral ptosis, ophthalmoparesis, mild facial weakness, nasal speech and high-arched palate (Fig. 1a, b). There was profound proximal and distal muscle weakness (2 to 3/5 MRC grade), and axial weakness of neck flexor and extensor (2/5 MRC grade) (Fig. 1c–e). Contractures of elbows, knees, and ankles were also noted, and deep tendon reflexes were absent. Creatine kinase (CK) levels were repeatedly within the normal range. Whole-body MRI revealed a significant involvement of the tongue, temporal muscles, lateral pterygoids and masseters with preservation of the medial pterygoids (supplementary Fig. S1a–s).

P2 is the first child born to healthy non-consanguineous parents. Neonatal and infancy periods were unremarkable, and initial concerns arose when the patient was unable to jump or run as fast as her peers at the age of 7 years. By 13 years of age she noticed difficulty ascending stairs, by 24 years of age she began using a walker, by 27 years of age she has been using a wheelchair for long distances, and by 32 years of age she noticed upper extremity proximal weakness. CK levels were repeatedly within the normal range. Examination at the age of 40 revealed symmetric, bilateral facial weakness with a transverse smile and minimal forehead movement, and a mildly high-arched palate. Ptosis or ophthalmoparesis were not noted. There was atrophy of the deltoids, the quadriceps, and the distal gastrocnemius muscles, with reduced strength in neck flexion, arm abduction, hip flexion, and hip extension (2/5 MRC grade), as well as in hip adduction (3/5 MRC grade). She was able to take steps independently with marked swaying (lateral leaning toward the leading leg). Deep tendon reflexes were reduced throughout the bilateral upper and lower extremities. There was evidence of spinal rigidity, mild thoracic scoliosis and mild contractures of the shoulders (on external rotation). Pulmonary function testing revealed a forced vital capacity (FVC) of 68% predicted upright and 65% predicted supine. Echocardiogram was normal. Lower extremity muscle MRI revealed atrophy, fatty infiltration and increased T1 signal throughout the muscles of the upper leg with relative sparing of the center of the rectus femoris muscles (Supplementary Fig. S1t, u). In the lower leg muscles, there was strikingly increased T1 signal of the soleus muscle bilaterally and the central portion of the medial gastrocnemius muscle on the left with evidence of fatty infiltration of the remaining muscles.

In summary, P1 and P2 presented with an early-onset and progressive myopathy clinically manifesting with significant muscle atrophy, facial weakness, contractures, and respiratory involvement, with a more severe disease progression and ocular involvement for P1.

Histochemical analyses revealed a unique circular arrangement of numerous small cores

P1 was biopsied twice at the age of 9 and 45 years, and P2 was biopsied at the age of 19 years. Histological analyses of the P1 deltoid muscle biopsy performed at 9 years of age revealed fiber size variability, type 1 fiber predominance, and single fibers with centralized

nuclei (Fig. 2a, b). Oxidative NADH-TR and SDH reactions uncovered an exceptional aspect of the intermyofibrillar network with numerous small cores often in apposition to each other, and sometimes forming a circular arrangement beneath the sarcolemma (Fig. 2a–d; arrows). These cores also appeared slightly darker on ATPase stain (Fig. 2b; arrow). Analysis of the P1 radialis muscle biopsy performed at 45 years of age confirmed marked fiber size variability and type 1 fiber predominance (95%), and also disclosed increased connective tissue (Fig. 2e, Supplementary Fig. S2a). Oxidative enzyme reactions revealed the presence of “cores” with sharp edges in type 1 fibers. Many fibers exhibited a diffuse structural disorganisation (Fig. 2f, Supplementary Fig. S2b), and scattered atrophic fibers were also observed (Fig. 2e, Supplementary Fig. S2a).

Histochemical analyses of the P2 quadriceps muscle biopsy performed at the age of 19 revealed striking similarities to the P1 deltoid muscle biopsy including the presence of internalized nuclei and numerous and peripheral small cores (Fig. 2g, h). Some protein aggregates were also observed (Supplementary Fig. S2c).

Taken together, P1 and P2 presented with similar clinical and histopathological features, and the remarkable arrangement of contiguous and subsarcolemmal cores was indicative of a new class of core myopathies.

Ultrastructural studies reveal jagged Z-lines with spiky edges

Electron microscopy of the P1 deltoid muscle biopsy performed at the age of 9 years uncovered numerous structured cores extending over a large number of sarcomeres, and spanning almost the whole width and length of the fibers. Within the cores, the Z-lines manifested a particular zigzag appearance to a greater or lesser extent. Centralized or internalized nuclei were also observed (Fig. 3a).

Ultrastructural analysis of the P1 radialis muscle biopsy performed at the age of 45 confirmed the presence of structured cores containing abnormal Z-lines. The jagged Z-lines gradually become serrated and merge into spiky edges of significant amplitude resembling a saw blade (Fig. 3b,c). The A and M bands were unaltered, and only the M band appeared slightly less marked (Fig. 3c). We also observed a number of fibers with internalized or pyknotic nuclei, as well as areas with sarcomeric bifurcation (Fig. 3b, c; arrow). On transverse muscle sections, numerous fibers showed areas of dispersed Z-line material (Supplementary Fig. S3), demonstrating a disruption of the myofibrillar organisation with preservation of the double square lattice of the Z-line [25]. Cross-sections through the sarcomere illustrated the normal regular distribution of the filaments forming a hexagonal lattice (Fig. 3d).

Identification of *de novo ACTN2* mutations

To identify the genetic cause of the muscle disorder, we performed exome sequencing on DNA samples from both index patients P1 and P2 and their unaffected family members (Fig. 4a,b). Following filtering and ranking of the datasets through our in-house bioinformatics pipeline [17], no pathogenic mutation in known muscle disorder genes was detected. Instead, we identified two *de novo* mutations in exon 18 of *ACTN2*: a heterozygous missense mutation in P1 (c.2180T>G, p.Leu727Arg), and a heterozygous in-frame deletion

of 33 nucleotides in P2 (c.2194_2226del; p.(Ala732_Ile742del)). None of the mutations was listed in the public gnomAD database quoting human DNA variants form almost 140 000 exomes and genomes, or in our in-house database containing more than 1500 exomes. The presence of the mutations in the patients, and the absence of the mutations in the healthy family members was confirmed by Sanger sequencing.

ACTN2 encodes alpha-actinin-2, which is composed of two actin-binding calponin-homology domains, a rod domain of four spectrin repeats in tandem, and two Ca^{2+}-binding EF-hands (Fig. 4c). The p.Leu727Arg substitution and the p.(Ala732_Ile742del) deletion affect conserved amino acids in the fourth spectrin repeat, and neither the nucleotide transversion nor the 33 nucleotides deletion is predicted to impact on splicing. Heterozygous *ACTN2* mutations were previously associated with cardiomyopathy [6, 18, 31, 44] (Fig. 4c). None of the eight reported cardiomyopathy mutations was found to reside within the fourth spectrin repeat, and none approximates the Leu727 and Ala732 to Ile742 residues on the resolved protein structure (Fig. 4c). In silico replacement of leucine 727 by arginine suggests that the arginine most probably interferes with neighboring amino acids, leading to steric hindrance (Fig. 4d). Arginine is also likely to alter the hydrophobic environment constituted by leucine 727 and the surrounding residues. The deletion from alanine 732 to isoleucine 742 is predicted to shorten a helix in the fourth spectrin repeat and may impact on the orientation of the structure. Moreover, as the p.(Ala732_Ile742)del deletion was identified after the completion of the following functional experiments, cell and animal work were focused on the p.Leu727Arg missense mutation.

The p.Leu727Arg mutation does not impact on alpha-actinin-2 stability, dimerization, and localization

To assess if the identified p.Leu727Arg mutation impacts on the alpha-actinin-2 level in the patient muscle, we performed immunoblotting. Western blot on muscle extracts revealed a comparable alpha-actinin-2 band of the expected size around 100 kDa in the P1 patient muscle and age-matched controls (Fig. 5a, supplementary Fig. S4), demonstrating that the *ACTN2* missense mutation has no major effect on splicing and does not significantly alter protein stability. We next assessed the potential impact of the p.Leu727Arg mutation on alpha-actinin-2 homodimerization. In transfected HeLa cells, wild-type alpha-actinin-2 comparably immunoprecipitated with wild-type and mutant alpha-actinin-2, demonstrating that the identified *ACTN2* mutation does not interfere with the protein dimerization properties (Supplementary Fig. S5).

Alpha-actinin-2 and alpha-actinin-3 are both expressed in human skeletal muscle, and it was previously shown that alpha-actinin-3 deficiency is compensated by *ACTN2* upregulation in both human and mouse [29, 35]. To investigate if the identified p.Leu727Arg mutation influences *ACTN3* expression, we probed alpha-actinin-3 through western blot on P1 muscle extracts. In contrast to the controls, no signal was detectable in the patient's muscle (Fig. 5b). *ACTN3* is however exclusively expressed in type 2 muscle fibers in humans, and the histopathological findings of type 1 fiber predominance in our patient most probably accounts for the absence of alpha-actinin-3 in the biopsy as P1 is heterozygous for the common *ACTN3* p.(Arg577*) variation.

Lastly, we assessed a potential impact of the p.Leu727Arg mutation on the intracellular alpha-actinin-2 localization in transfected cells. In differentiated C2C12 muscle cells, both wild-type and mutant alpha-actinin-2 were found to form a striated pattern consistent with a Z-line localization (Fig. 5c). We also observed a normal co-localization of the known alpha-actinin-2 interactors vinculin and actin in myoblasts, at the focal adhesion and stress fibers respectively (Supplementary Fig. S6a,b).

Taken together, our protein studies suggest that the p.Leu727Arg mutation does not significantly impact on *ACTN2* mRNA splicing, and does not affect the stability or the intracellular localization of alpha-actinin-2.

The p.Leu727Arg mutation severely impairs zebrafish muscle structure and function

Human leucine 727 is highly conserved in all vertebrate species. To evaluate the physiological impact of the alpha-actinin-2 p.Leu727Arg mutation on skeletal muscle structure and function, we performed overexpression experiments in the zebrafish model. *ACTN2* wild-type mRNA injected fish were indistinguishable from uninjected controls. In contrast, injection of mutant human *ACTN2* mRNA into 1-cell zebrafish embryos resulted in smaller myotome and dorsal curvature (phenotype scored in Fig. 6a,b). Western blot analysis showed equal levels of wild-type and p.Leu727Arg alpha-actinin-2 in zebrafish larvae (3dpf) (Supplementary Fig. S7). While healthy developing zebrafish embryos typically hatch from their protective chorions by 2–2.5 dpf (97.2 ± 1%), only a small fraction of p.Leu727Arg-injected zebrafish hatched from their chorion (12.6 ± 7%, $p<0.05$) and required manual dechorionation for imaging, demonstrating early motor defects. Hatching defects were also reported in other zebrafish models of muscle diseases and reflect early motor defects [43]. Birefringence assays on axial skeletal muscles of live zebrafish embryos showed a reduction in birefringence only in zebrafish injected with p.Leu727Arg mRNA (Fig. 6a). The motor function was quantified by measuring the total distance travelled by control, wild-type and mutant mRNA-injected fish. Zebrafish expressing p.Leu727Arg alpha-actinin-2 displayed a significant reduction in the total swimming distance (724.6 ± 83.3 mm) in comparison to the wild-type injected fish (2489.2 ± 119.1 mm) or uninjected controls (2411.4 ± 94.7 mm), demonstrating a mutational impact on muscle function (Fig. 6c).

We also examined the skeletal muscle architecture of the injected zebrafish. Whole-mount immunostaining with phalloidin revealed a close proximity of adjacent myofibers in the controls, whereas p.Leu727Arg-injected zebrafish exhibited gaps between overall smaller myofibers (Fig. 7a). To identify potential ultrastructural defects in subcellular compartments of skeletal muscle, we performed transmission electron microscopy at 3 dpf. Longitudinal muscle sections showed significant myofibrillar disarray lacking normal actin-myosin organization in p.Leu727Arg-injected zebrafish as compared to the highly organized myofibrillar structure in *ACTN2* wild-type injected or uninjected control zebrafish (Fig. 7b). In accordance with the findings on the patient muscle biopsies, the myofibers of p.Leu727Arg-injected fish showed areas with abnormal Z-lines.

The p.Leu727Arg mutation induces structured cores and causes muscle weakness in mice

To further validate and characterize the impact of the alpha-actinin-2 p.Leu727Arg mutation on muscle function at later stages of muscle development and in a different model, we performed AAV-mediated *ACTN2* overexpression in 3 weeks-old mice and analyzed muscle force and muscle structure 4 weeks post injection. Tibialis anterior muscles injected with wild-type or mutant human *ACTN2* showed a twofold increased alpha-actinin-2 level as compared to control muscles injected with empty AAV (Fig. 8a), while the alpha-actinin-3 and actin levels remained unchanged (Supplementary Fig. S8a,b). Using a force transducer, we detected a significantly reduced maximal and specific force of p.Leu727Arg-injected tibialis anterior compared to muscles injected with empty AAV or wild-type *ACTN2* respectively (Fig. 8b–d).

Immunofluorescence on longitudinal tibialis anterior sections demonstrated an abnormal Z-line organization in muscles injected with mutant *ACTN2* (Fig. 8e). Histochemical analyses on transversal muscle sections from mice expressing mutant *ACTN2* revealed the presence of cores (Fig. 9a,b, Supplementary Fig. S9), while none of these features was observed in the AAV-empty and AAV-*ACTN2* wild-type injected controls. We further investigated the muscle structure by electron microscopy, and we detected an abnormal Z-line architecture in tibialis anterior expressing p.Leu727Arg alpha-actinin-2 but not in the controls (Fig. 10). The Z-lines in p.Leu727Arg injected tibialis anterior were enlarged with a zigzag appearance, and were sometimes split (Fig. 10d), in accordance to zebrafish muscles expressing the p.Leu727Arg alpha-actinin-2 and to the histopathological observations on the patient's biopsies.

In summary, the mouse and zebrafish models recapitulated the structural defects observed in the P1 biopsies with strikingly jagged Z-lines, and both animal models manifested muscle weakness, representing the main clinical feature in the patients with *ACTN2* mutations.

Discussion

This study describes a congenital myopathy characterized by multiple structured cores and distinctive jagged-Z-lines in muscle fibers caused by dominant *ACTN2* mutations. We provide clinical, histological, ultrastructural, and genetic data, and evidence the pathogenicity of the missense mutation through muscle function experiments in zebrafish and mouse models.

A unique core myopathy: clinical, histological, and ultrastructural hallmarks

Both patients presented with early-onset muscle weakness and a progressive course of disease resulting in partial or complete loss of ambulation. P1 presented with a more severe disease progression with an additional ocular involvement. Clinical heterogeneity has frequently been described in patients with congenital myopathies and may relate to the genetic background or non-genetic environmental effects. Muscle biopsies from both patients revealed a highly similar picture with type 1 fiber predominance and multiple structured cores forming a circular arrangement beneath the sarcolemma. Predominance of type 1 fibers is a frequent feature in congenital myopathies and may contribute to the muscle

weakness in combination with the overall reduced expression of alpha-actinin-3, a type 2-specific muscle function modifier. A detailed ultrastructural comparison of both P1 biopsies performed in childhood and adulthood suggested a progression of the lesions, as the degree of Z-line jagging was distinctively more pronounced in the second biopsy and taking an aspect of a saw blade. In CCD, structured or unstructured cores are usually unique with a central or eccentric position. In some cases, two or even three cores may coexist in the same fiber, but never contiguously. It should be noted that abnormal or multiple sarcoplasmic reticular triads are frequently found at their periphery [40]. In MmD, the cores are boundless, smaller, encompassing only a few sarcomeres, and the disorganized filaments present a rather transversal orientation. Minicores can also be found in healthy muscle following reactive exercise [16] or after muscle injury, and they are only considered as pathogenic if found in great numbers and exclusively in type I fibers. Taking into account the unique histopathology of multiple structured and contiguous cores in the biopsy of our patients, we propose the term “Multiple structured Core Disease” (MsCD) to describe this novel entity in the group of core myopathies.

ACTN2 mutations: cardiomyopathy vs myopathy

Alpha-actinin-2 is expressed in skeletal and cardiac muscle [2], and heterozygous *ACTN2* mutations have previously been associated with hypertrophic or dilated cardiomyopathy, without any reported motor or skeletal muscle involvement. To date, eight mutations were reported, and all are missense mutations affecting conserved amino acids [6, 18, 31, 44]. The mutations are evenly distributed and found in the calponin-homology domains, as well as in some spectrin repeats and in the EF-hands. The spectrin domain mutations p.Thr495Met and p.Glu628Gly were thereby found in spectrin domains 2 and 3, respectively. A subset of the cardiomyopathy-related *ACTN2* mutations have been investigated experimentally. The very N-terminal p.Gln9Arg mutation was shown to disrupt the interaction with the muscle LIM protein, and the calponin-homology domain mutations p.Gly11Val and p.Ala119thr interfered with actin binding [22]. The resolved protein structure of alpha-actinin-2 shows that none of the cardiomyopathy-related mutations affects residues in close proximity to the myopathy-related alpha-actinin-2 mutations described here. Moreover, leucine 727 and alanine 732 to isoleucine

742 reside within the same alpha-helix and replacement by arginine or deletion of 11 amino acids may have different chemical and/or structural impacts compared to the cardiomyopathy mutations, and thereby underlies the diverging pathomechanisms resulting in either skeletal muscle or a cardiac disorder. We can however not exclude that the myopathy-related p.Leu727Arg or p.(Ala732_Ile742del) mutations might also result in cardiac involvement at later stages or on a different genetic background. It should be noted that P1 manifested cardiac insufficiency in the neonatal period that disappeared by the age of 6 months following symptomatic treatment.

Insight into the pathogenesis

Through exome sequencing, we identified the *de novo ACTN2* c.2180T>G (p.Leu727Arg) and c.2194_2226del (p.(Ala732_Ile742del)) mutations as the genetic cause of MsCD. *ACTN2* is highly expressed in skeletal muscle, and the identified mutations are not listed in

the SNP databases. The pathogenicity of the *ACTN2* mutations can be inferred from the patient analyses and our animal experimentation results. It has previously been shown that alpha-actinin-2 deficiency results in sarcomeric defects in zebrafish [19], demonstrating the essential role of alpha-actinin-2 in the integrity of the contractile apparatus in skeletal muscle. Here we exogenously expressed human p.Leu727Arg *ACTN2*, and the injected zebrafish manifested both functional and structural muscle defects including abnormal Z-lines. We also performed AAV-mediated human *ACTN2* overexpression in murine tibialis anterior, and the muscles injected with the p.Leu727Arg construct developed less force than the controls and displayed cores and jagged Z-lines. Taken together, the animal models recapitulated the major muscle features of human *ACTN2*-related myopathy at both the clinical and the histological level. Moreover, both animal models provide faithful tools to investigate further therapeutic approaches. Our cell experiments disclosed that the Z-line protein alpha-actinin-2 p.Leu727Arg forms a striated pattern as expected and still binds the tested interactors. The abnormal Z-line architecture observed in the P1 muscle biopsy and in the animal models however demonstrates that the p.Leu727Arg mutation impacts on the integrity of the Z-line, potentially through untested or unknown function/interactors. The disease progression might thereby result from the accumulative mechanical stress acting on the Z-line over time, leading to the abnormal Z-line architecture, and representing the main reason for the progressive muscle weakness observed in the patients.

Conclusions

Here we describe a unique congenital myopathy at the clinical, histological, morphological, and genetic level. We identified the first *ACTN2* mutations associated with Multiple structured Core disease (MsCD), characterized by unique and distinctive histological features including numerous contiguous structured cores and jagged Z-lines with spiky edges, and we demonstrated pathogenicity in zebrafish and mouse. This work provides insight into pathogenic alterations of the Z-line architecture and will improve the molecular diagnosis for patients with rare muscle disorders.

Supplementary Material

Refer to Web version on PubMed Central for supplementary material.

Acknowledgements

We thank the families for their participation in the study. We also thank Valentina Lionello, Loïc Talide, Suzie Buono, Coralie Spiegelhalter, Bruno Weber and Pascale Koebel for technical assistance, Jahannaz Dastgir, Katherine Meilleur, Neal Busis, Lauren Elman, Xilma Ortiz-Gonzalez, and Henry Wessel for their help with patient care, and Susana Quijano-Roy, Christopher Mendoza and Gilberto Averion for their help in clinic. We also would like to thank the Exome Aggregation Consortium and the groups that provided exome variant data for comparison. A full list of contributing groups can be found at http://exac.broadinstitute.org/about.

Funding

This work was funded by the Institut National de la Santé et de la Recherche Médicale (INSERM), Centre National de la Recherche Scientifique (CNRS), University of Strasbourg, GIS IBiSA maladies rares, the France Génomique National infrastructure funded as part of the Investissements d'Avenir program managed by the Agence Nationale pour la Recherche (ANR-10-INBS-09) and by Fondation Maladies Rares within the frame of the "Myocapture" sequencing project, the Fondation pour la Recherche Médicale, and the Association Française contre les Myopathies. The work performed at the NIH was supported by intramural funds from the NIH National Institute of

Neurological Disorders and Stroke. Sequencing analysis was provided by the Broad Institute of MIT and Harvard Center for Mendelian Genomics and was funded by the National Human Genome Research Institute, the National Eye Institute and the National Heart, Lung and Blood Institute grant UM1 HG008900 to Daniel MacArthur and Heidi Rehm.

References

1. Bang ML, Mudry RE, McElhinny AS, Trombitas K, Geach AJ, Yamasaki R, Sorimachi H, Granzier H, Gregorio CC, Labeit S (2001) Myopalladin, a novel 145-kilodalton sarcomeric protein with multiple roles in Z-disc and I-band protein assemblies. J Cell Biol 153: 413–427 [PubMed: 11309420]
2. Beggs AH, Byers TJ, Knoll JH, Boyce FM, Bruns GA, Kunkel LM (1992) Cloning and characterization of two human skeletal muscle alpha-actinin genes located on chromosomes 1 and 11. J Biol Chem 267: 9281–9288 [PubMed: 1339456]
3. Bennett AH, O'Donohue MF, Gundry SR, Chan AT, Widrick J, Draper I, Chakraborty A, Zhou Y, Zon LI, Gleizes PE et al (2018) RNA helicase, DDX27 regulates skeletal muscle growth and regeneration by modulation of translational processes. PLoS Genet 14: e1007226 Doi 10.1371/journal.pgen.1007226
4. Carlier R (2014) MNM et IRM musculaire/corps entier : apport au diagnostic et au suivi. In: AFM-Téléthon, Société Française de Myologie SFM (eds) Les Cahiers de Myologie, pp 22–32
5. Chan Y, Tong HQ, Beggs AH, Kunkel LM (1998) Human skeletal muscle-specific alpha-actinin-2 and −3 isoforms form homodimers and heterodimers in vitro and in vivo. Biochem Biophys Res Commun 248: 134–139 [PubMed: 9675099]
6. Chiu C, Bagnall RD, Ingles J, Yeates L, Kennerson M, Donald JA, Jormakka M, Lind JM, Semsarian C (2010) Mutations in alpha-actinin-2 cause hypertrophic cardiomyopathy: a genome-wide analysis. J Am Coll Cardiol 55: 1127–1135 Doi 10.1016/j.jacc.2009.11.016 [PubMed: 20022194]
7. Cowling BS, Toussaint A, Amoasii L, Koebel P, Ferry A, Davignon L, Nishino I, Mandel JL, Laporte J (2011) Increased expression of wild-type or a centronuclear myopathy mutant of dynamin 2 in skeletal muscle of adult mice leads to structural defects and muscle weakness. Am J Pathol 178: 2224–2235 Doi 10.1016/j.ajpath.2011.01.054 [PubMed: 21514436]
8. Cukovic D, Lu GW, Wible B, Steele DF, Fedida D (2001) A discrete amino terminal domain of Kv1.5 and Kv1.4 potassium channels interacts with the spectrin repeats of alpha-actinin-2. FEBS Lett 498: 87–92 [PubMed: 11389904]
9. Dubowitz V, Pearse AG (1960) Oxidative enzymes and phosphorylase in central-core disease of muscle. Lancet 2: 23–24 [PubMed: 13818365]
10. Dunbrack RL Jr., (2002) Rotamer libraries in the 21st century. Curr Opin Struct Biol 12: 431–440 [PubMed: 12163064]
11. Eilertsen KJ, Kazmierski ST, Keller TC 3rd, (1997) Interaction of alpha-actinin with cellular titin. Eur J Cell Biol 74: 361–364 [PubMed: 9438132]
12. Engel AG, Gomez MR, Groover RV (1971) Multicore disease. A recently recognized congenital myopathy associated with multifocal degeneration of muscle fibers. Mayo Clin Proc 46: 666–681 [PubMed: 5115748]
13. Fardeau M (1982) Congenital Myopathies In: Mastaglia F, Walton J (eds) Skeletal Muscle Pathology 2nd edn Churchill Livingstone, Edinburgh, pp 237–281
14. Ferreiro A, Estournet B, Chateau D, Romero NB, Laroche C, Odent S, Toutain A, Cabello A, Fontan D, dos Santos HG et al (2000) Multi-minicore disease--searching for boundaries: phenotype analysis of 38 cases. Ann Neurol 48: 745–757 [PubMed: 11079538]
15. Finn RD, Attwood TK, Babbitt PC, Bateman A, Bork P, Bridge AJ, Chang HY, Dosztanyi Z, El-Gebali S, Fraser M et al (2017) InterPro in 2017-beyond protein family and domain annotations. Nucleic Acids Res 45: D190–D199 Doi 10.1093/nar/gkw1107 [PubMed: 27899635]
16. Friden J, Sjostrom M, Ekblom B (1983) Myofibrillar damage following intense eccentric exercise in man. Int J Sports Med 4: 170–176 [PubMed: 6629599]

17. Geoffroy V, Pizot C, Redin C, Piton A, Vasli N, Stoetzel C, Blavier A, Laporte J, Muller J (2015) VaRank: a simple and powerful tool for ranking genetic variants. PeerJ 3: e796 Doi 10.7717/peerj.796 [PubMed: 25780760]

18. Girolami F, Iascone M, Tomberli B, Bardi S, Benelli M, Marseglia G, Pescucci C, Pezzoli L, Sana ME, Basso Cet al (2014) Novel alpha-actinin 2 variant associated with familial hypertrophic cardiomyopathy and juvenile atrial arrhythmias: a massively parallel sequencing study. Circ Cardiovasc Genet 7: 741–750 Doi 10.1161/CIRCGENETICS.113.000486 [PubMed: 25173926]

19. Gupta V, Discenza M, Guyon JR, Kunkel LM, Beggs AH (2012) alpha-Actinin-2 deficiency results in sarcomeric defects in zebrafish that cannot be rescued by alpha-actinin-3 revealing functional differences between sarcomeric isoforms. FASEB J 26: 1892–1908 Doi 10.1096/fj.11-194548 [PubMed: 22253474]

20. Hall DD, Dai S, Tseng PY, Malik Z, Nguyen M, Matt L, Schnizler K, Shephard A, Mohapatra DP, Tsuruta Fet al (2013) Competition between alpha-actinin and Ca(2)(+)-calmodulin controls surface retention of the L-type Ca(2)(+) channel Ca(V)1.2. Neuron 78: 483–497 Doi 10.1016/j.neuron.2013.02.032 [PubMed: 23664615]

21. Hance JE, Fu SY, Watkins SC, Beggs AH, Michalak M (1999) alpha-actinin-2 is a new component of the dystrophin-glycoprotein complex. Arch Biochem Biophys 365: 216–222 Doi 10.1006/abbi.1999.1172 [PubMed: 10328815]

22. Haywood NJ, Wolny M, Rogers B, Trinh CH, Shuping Y, Edwards TA, Peckham M (2016) Hypertrophic cardiomyopathy mutations in the calponin-homology domain of ACTN2 affect actin binding and cardiomyocyte Z-disc incorporation. Biochem J 473: 2485–2493 Doi 10.1042/BCJ20160421 [PubMed: 27287556]

23. Huang SM, Huang CJ, Wang WM, Kang JC, Hsu WC (2004) The enhancement of nuclear receptor transcriptional activation by a mouse actin-binding protein, alpha actinin 2. J Mol Endocrinol 32: 481–496 [PubMed: 15072553]

24. Kimmel CB, Ballard WW, Kimmel SR, Ullmann B, Schilling TF (1995) Stages of embryonic development of the zebrafish. Dev Dyn 203: 253–310 Doi 10.1002/aja.1002030302 [PubMed: 8589427]

25. Landon D (1982) Skeletal muscle - normal morphology, development and innervation. In: Mastaglia F, Walton J (eds) Skeletal muscle pathology Churchill Livingstone, Edinburgh, pp 1–87

26. Linke WA, Ivemeyer M, Labeit S, Hinssen H, Ruegg JC, Gautel M (1997) Actin-titin interaction in cardiac myofibrils: probing a physiological role. Biophys J 73: 905–919 Doi 10.1016/S0006-3495(97)78123-2 [PubMed: 9251807]

27. Liu W, Xie Y, Ma J, Luo X, Nie P, Zuo Z, Lahrmann U, Zhao Q, Zheng Y, Zhao Y et al (2015) IBS: an illustrator for the presentation and visualization of biological sequences. Bioinformatics 31: 3359–3361 Doi 10.1093/bioinformatics/btv362 [PubMed: 26069263]

28. Lu L, Timofeyev V, Li N, Rafizadeh S, Singapuri A, Harris TR, Chiamvimonvat N (2009) Alpha-actinin2 cytoskeletal protein is required for the functional membrane localization of a Ca2+-activated K+ channel (SK2 channel). Proc Natl Acad Sci U S A 106: 18402–18407 Doi 10.1073/pnas.0908207106 [PubMed: 19815520]

29. MacArthur DG, Seto JT, Chan S, Quinlan KG, Raftery JM, Turner N, Nicholson MD, Kee AJ, Hardeman EC, Gunning PWet al (2008) An Actn3 knockout mouse provides mechanistic insights into the association between alpha-actinin-3 deficiency and human athletic performance. Hum Mol Genet 17: 1076–1086 Doi 10.1093/hmg/ddm380 [PubMed: 18178581]

30. McGregor A, Blanchard AD, Rowe AJ, Critchley DR (1994) Identification of the vinculin-binding site in the cytoskeletal protein alpha-actinin. Biochem J 301 (Pt 1): 225–233 [PubMed: 8037676]

31. Mohapatra B, Jimenez S, Lin JH, Bowles KR, Coveler KJ, Marx JG, Chrisco MA, Murphy RT, Lurie PR, Schwartz RJ et al (2003) Mutations in the muscle LIM protein and alpha-actinin-2 genes in dilated cardiomyopathy and endocardial fibroelastosis. Mol Genet Metab 80: 207–215 [PubMed: 14567970]

32. Murphy AC, Young PW (2015) The actinin family of actin cross-linking proteins - a genetic perspective. Cell Biosci 5: 49 Doi 10.1186/s13578-015-0029-7 [PubMed: 26312134]

33. Nance JR, Dowling JJ, Gibbs EM, Bonnemann CG (2012) Congenital myopathies: an update. Curr Neurol Neurosci Rep 12: 165–174 Doi 10.1007/s11910-012-0255-x [PubMed: 22392505]

34. Nave R, Furst DO, Weber K (1990) Interaction of alpha-actinin and nebulin in vitro. Support for the existence of a fourth filament system in skeletal muscle. FEBS Lett 269: 163–166 [PubMed: 2387397]
35. North KN, Yang N, Wattanasirichaigoon D, Mills M, Easteal S, Beggs AH (1999) A common nonsense mutation results in alpha-actinin-3 deficiency in the general population. Nat Genet 21: 353–354 Doi 10.1038/7675 [PubMed: 10192379]
36. Otey CA, Pavalko FM, Burridge K (1990) An interaction between alpha-actinin and the beta 1 integrin subunit in vitro. J Cell Biol 111: 721–729 [PubMed: 2116421]
37. Pettersen EF, Goddard TD, Huang CC, Couch GS, Greenblatt DM, Meng EC, Ferrin TE (2004) UCSF Chimera--a visualization system for exploratory research and analysis. J Comput Chem 25: 1605–1612 Doi 10.1002/jcc.20084 [PubMed: 15264254]
38. Ribeiro Ede A Jr., Pinotsis N, Ghisleni A, Salmazo A, Konarev PV, Kostan J, Sjoblom B, Schreiner C, Polyansky AA, Gkougkoulia EA et al (2014) The structure and regulation of human muscle alpha-actinin. Cell 159: 1447–1460 Doi 10.1016/j.cell.2014.10.056 [PubMed: 25433700]
39. Robison AJ, Bass MA, Jiao Y, MacMillan LB, Carmody LC, Bartlett RK, Colbran RJ (2005) Multivalent interactions of calcium/calmodulin-dependent protein kinase II with the postsynaptic density proteins NR2B, densin-180, and alpha-actinin-2. J Biol Chem 280: 35329–35336 Doi 10.1074/jbc.M502191200 [PubMed: 16120608]
40. Romero NB, Clarke NF (2013) Congenital myopathies. Handb Clin Neurol 113: 1321–1336 Doi 10.1016/B978-0-444-59565-2.00004-6 [PubMed: 23622357]
41. Salmikangas P, Mykkanen OM, Gronholm M, Heiska L, Kere J, Carpen O (1999) Myotilin, a novel sarcomeric protein with two Ig-like domains, is encoded by a candidate gene for limb-girdle muscular dystrophy. Hum Mol Genet 8: 1329–1336 [PubMed: 10369880]
42. Sewry CA, Wallgren-Pettersson C (2017) Myopathology in congenital myopathies. Neuropathol Appl Neurobiol 43: 5–23 Doi 10.1111/nan.12369
43. Smith SJ, Wang JC, Gupta VA, Dowling JJ (2017) A novel early onset phenotype in a zebrafish model of merosin deficient congenital muscular dystrophy. Plos One 12: e0172648 Doi 10.1371/journal.pone.0172648
44. Theis JL, Bos JM, Bartleson VB, Will ML, Binder J, Vatta M, Towbin JA, Gersh BJ, Ommen SR, Ackerman MJ (2006) Echocardiographic-determined septal morphology in Z-disc hypertrophic cardiomyopathy. Biochem Biophys Res Commun 351: 896–902 Doi 10.1016/j.bbrc.2006.10.119 [PubMed: 17097056]
45. Westerfield M (2007) The Zebrafish Book: A Guide for the Laboratory Use of Zebrafish (Danio Rerio). City
46. Wyszynski M, Lin J, Rao A, Nigh E, Beggs AH, Craig AM, Sheng M (1997) Competitive binding of alpha-actinin and calmodulin to the NMDA receptor. Nature 385: 439–442 Doi 10.1038/385439a0 [PubMed: 9009191]

Fig. 1.

Photographs of P1 **a** Mild bilateral ptosis. **b** High-arched palate. **c** Upper extremity hypotrophy and pectus excavatum. **d** Residual arm flexors force. **e** Profound leg weakness

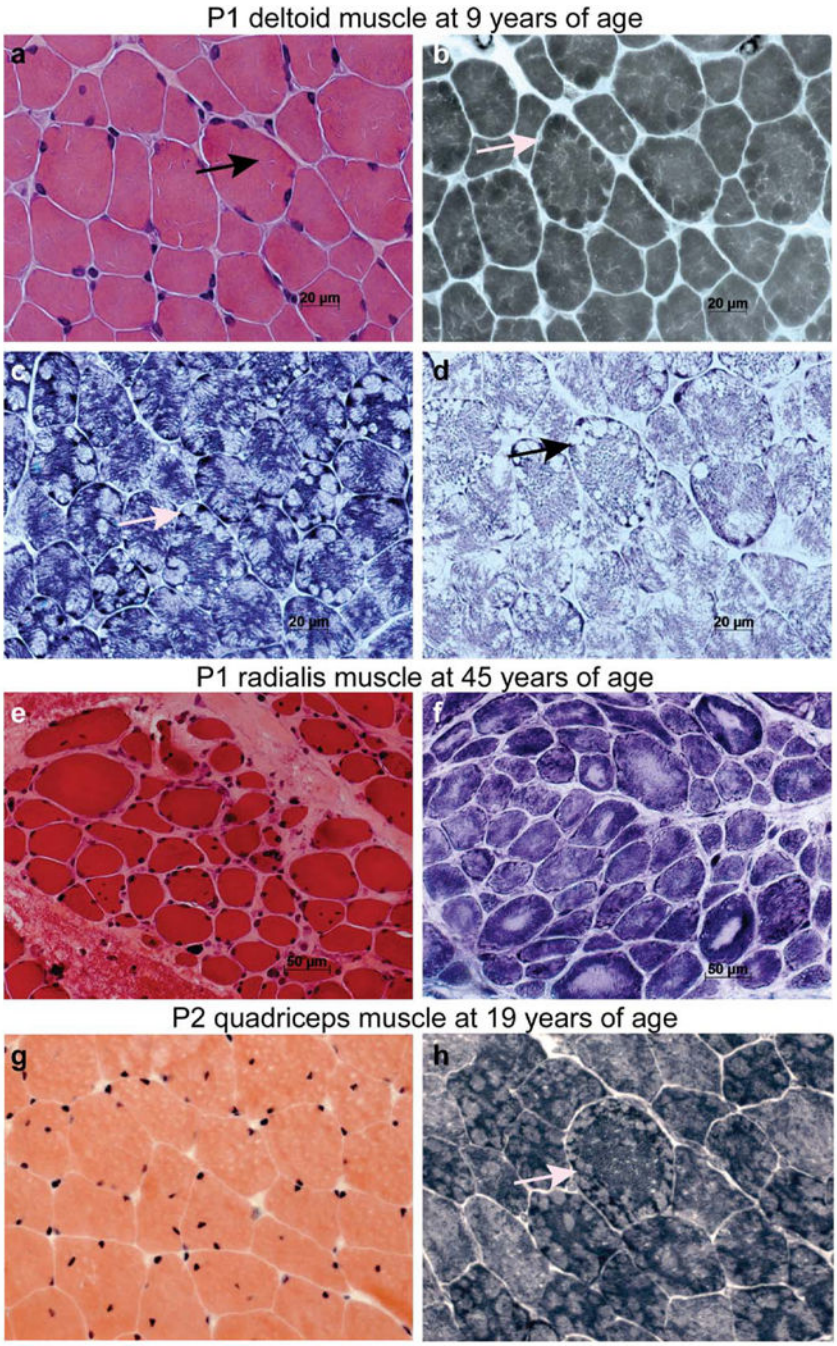

Fig. 2.

Skeletal muscle histopathology of P1 at 9 and 45 years, and P2 at 19 years of age. P1 transversal muscle sections from the deltoid biopsy performed at 9 years of age (a,b,c,d) and from the radialis muscle biopsy performed at 45 years of age (e,f). **a** HE staining reveals fiber size variability, centralized nuclei, and cores (black arrow). **b** ATP staining (pH 9.4) shows type 1 fiber predominance. The subsarcolemmal cores appear slightly darker (arrow). **c, d** NADH and SDH reactions unravel numerous small cores in a circular arrangement beneath the sarcolemma (arrows). **e** HE staining confirms fiber size variability and nuclear

internalization, and reveals an increase of connective tissue. **f** NADH shows numerous muscle fibers with well-delimited cores and a diffuse structural disorganisation in several fibers. P2 transversal sections from the quadriceps biopsy performed at 19 years of age (g,h). **g** HE staining revealed internalized nuclei. **h** NADH reactions demonstrated several small cores mainly located at the periphery of the fibers

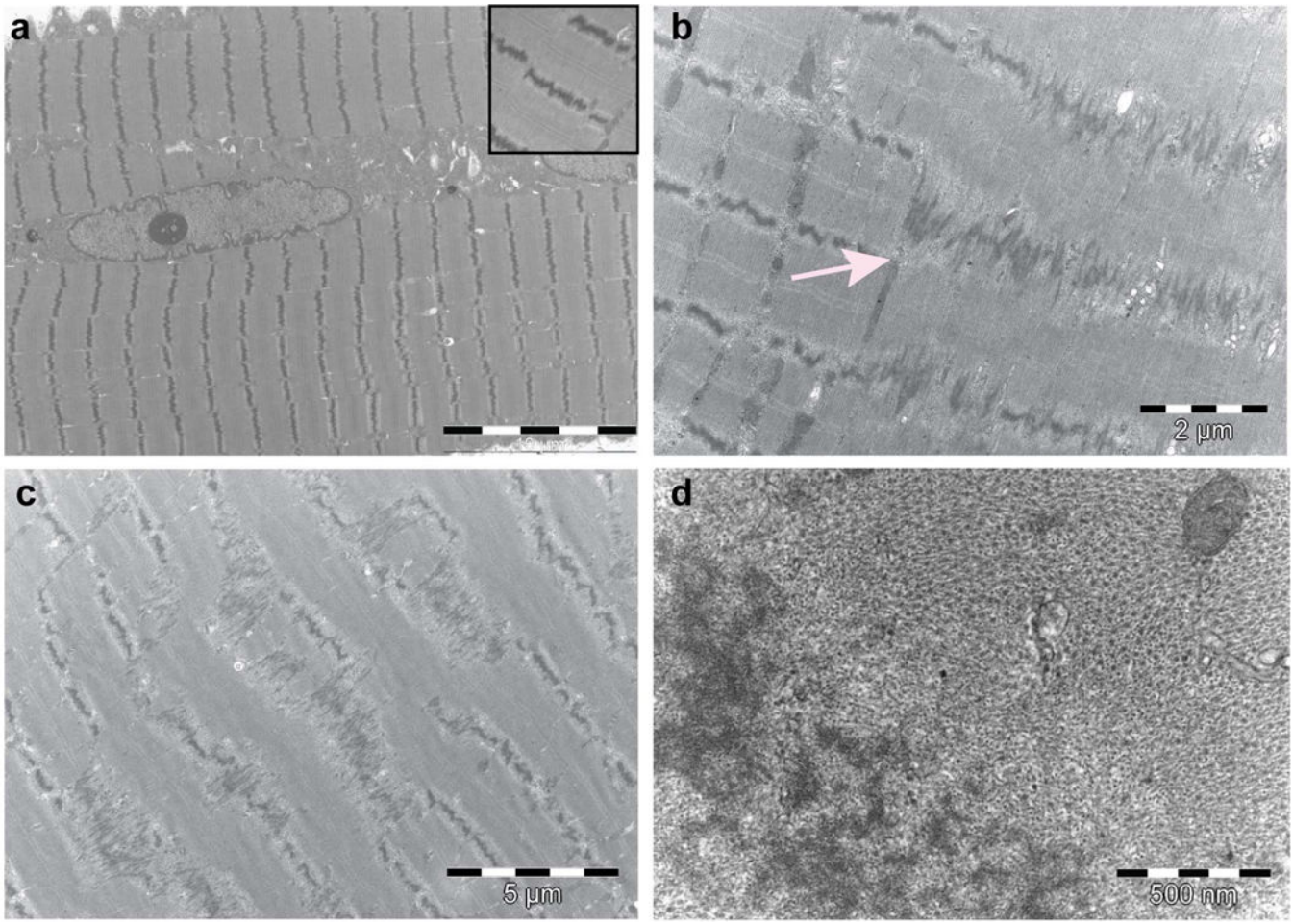

Fig. 3.

Progressive ultrastructural muscle alterations of patient P1. Longitudinal muscle sections of the deltoid biopsy (a) and the radialis biopsy (b,c), and transversal sections of the radialis biopsy (d). **a** The muscle fiber is fully occupied with structured cores, one next to the other, which extend almost along the full length of the fibers. Electron microscopy of the cores shows centralized nuclei and Z-lines with zigzag appearance (zoom on the top right corner). **b,c** Bifurcation and transition of zigzag Z-lines towards jagged Z-lines with sharp edges resembling a saw blade in contiguous myofibrils (arrow). **d** High-magnification image showing the scattering of Z-line material at different points. Note however the normal regular distribution of filaments which form a typical hexagonal lattice

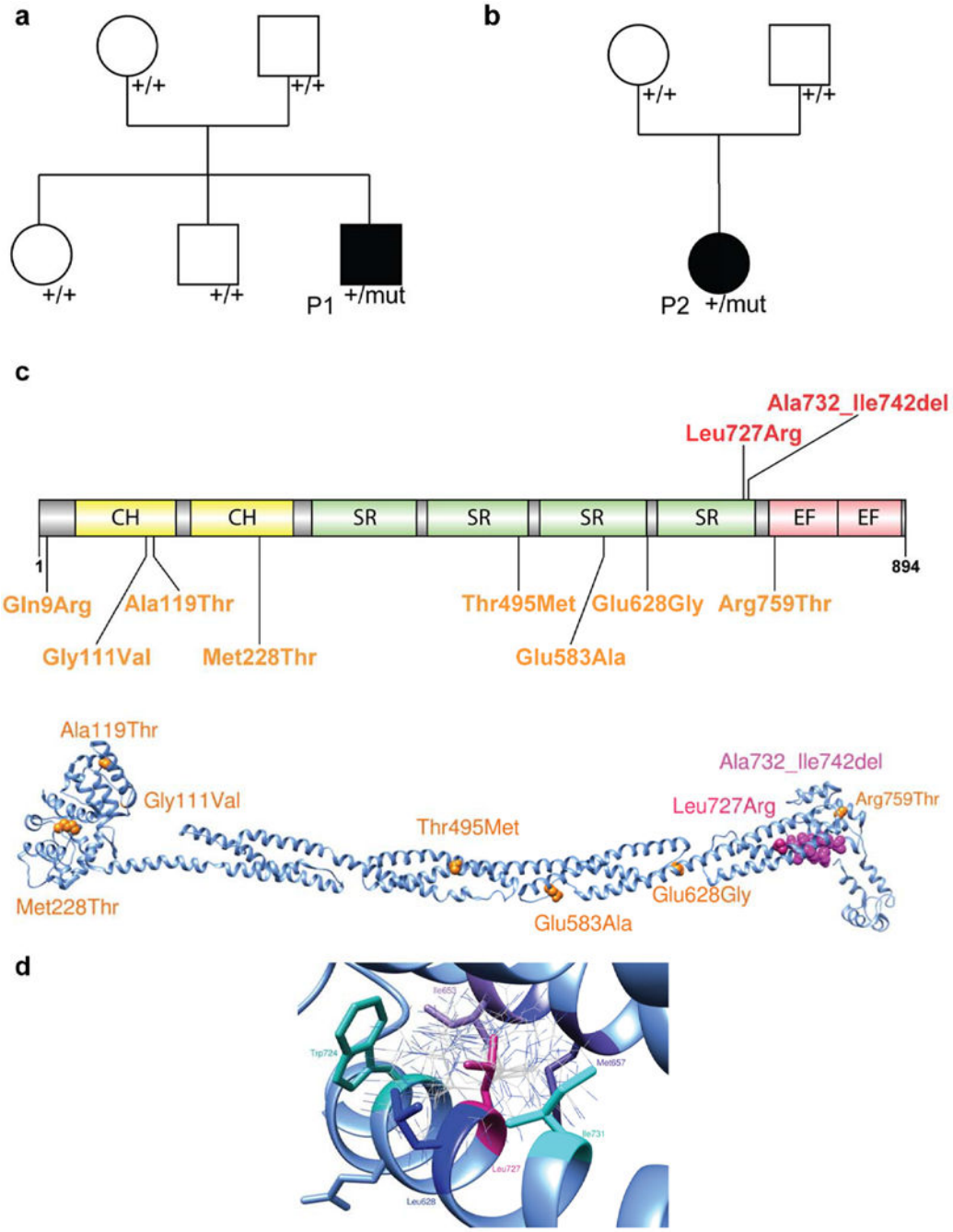

Fig. 4.

ACTN2 mutations. **a, b** Pedigrees of the families with *de novo ACTN2* missense mutations. **c** Representation of alpha-actinin-2 domains and structure (PDB 4D1E) showing the position of the novel mutations (in pink or red) and of the mutations previously described in cardiomyopathies (in orange). **d** Prediction of the replacement of leucine 727 (in pink) by arginine in the 3D structure of alpha-actinin-2. All rotamers (possible conformations) of arginine at position 727 were added to the wild-type structure to illustrate the potential interference with the neighbouring residues. Neighbouring hydrophic residues are in cyan

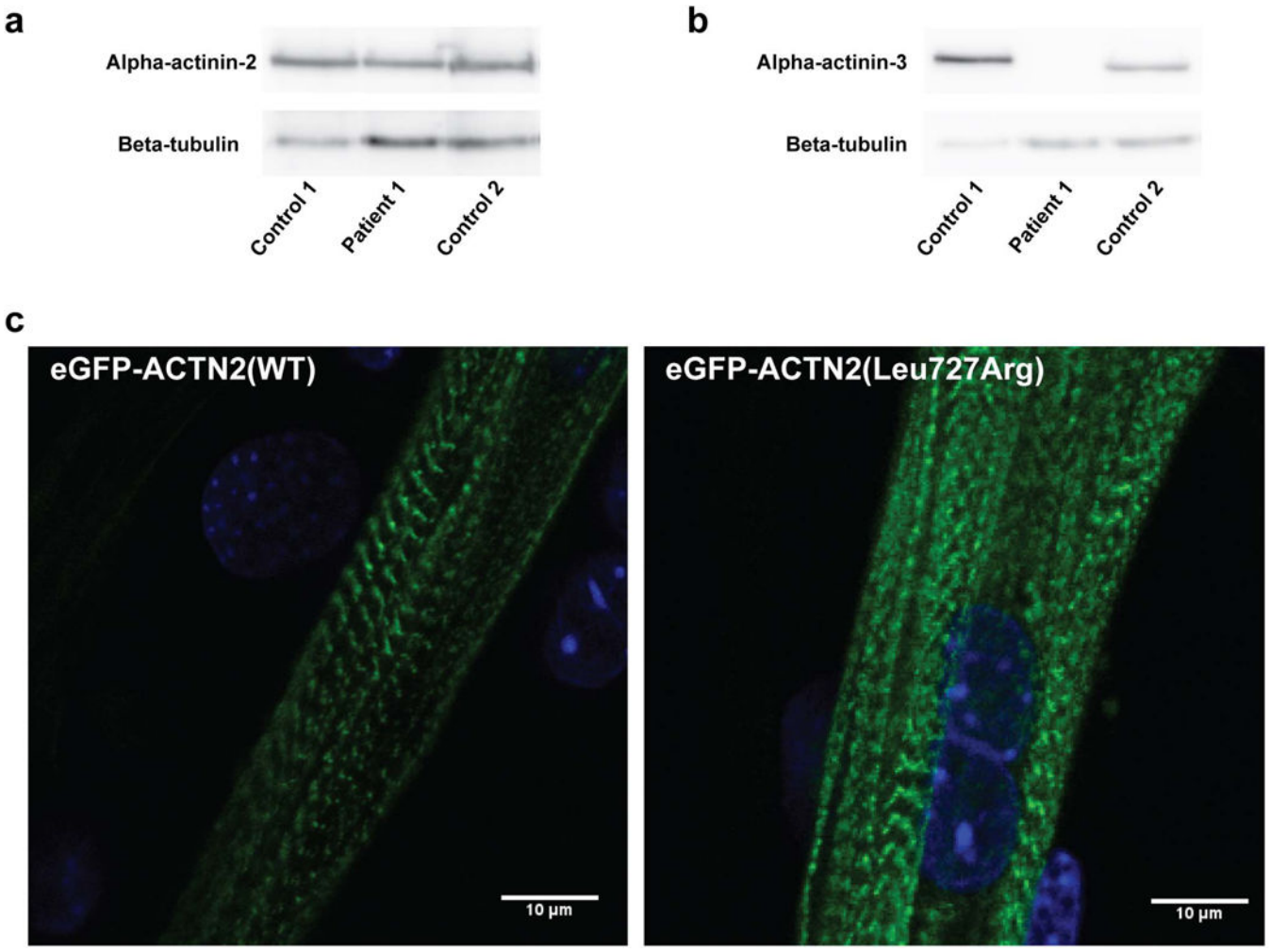

Fig. 5.

Impact of the *ACTN2* p.Leu727Arg mutation on protein stability and localization. **a** SDS-Page of age-matched controls and patient muscle protein extracts probed with antibodies against alpha-actinin-2 and anti-beta-tubulin showed bands of similar size and signal intensity. **b** SDS-Page of age-matched controls and patient P1 muscle protein extracts revealed with antibodies against alpha-actinin-3 and beta-tubulin showed strong reduction of alpha-actinin-3 in the patient's biopsy. **c** Comparable localization of eGFP-alpha-actinin-2 wild-type and mutant in transfected and differentiated C2C12 myotubes (day 8 after start of differentiation)

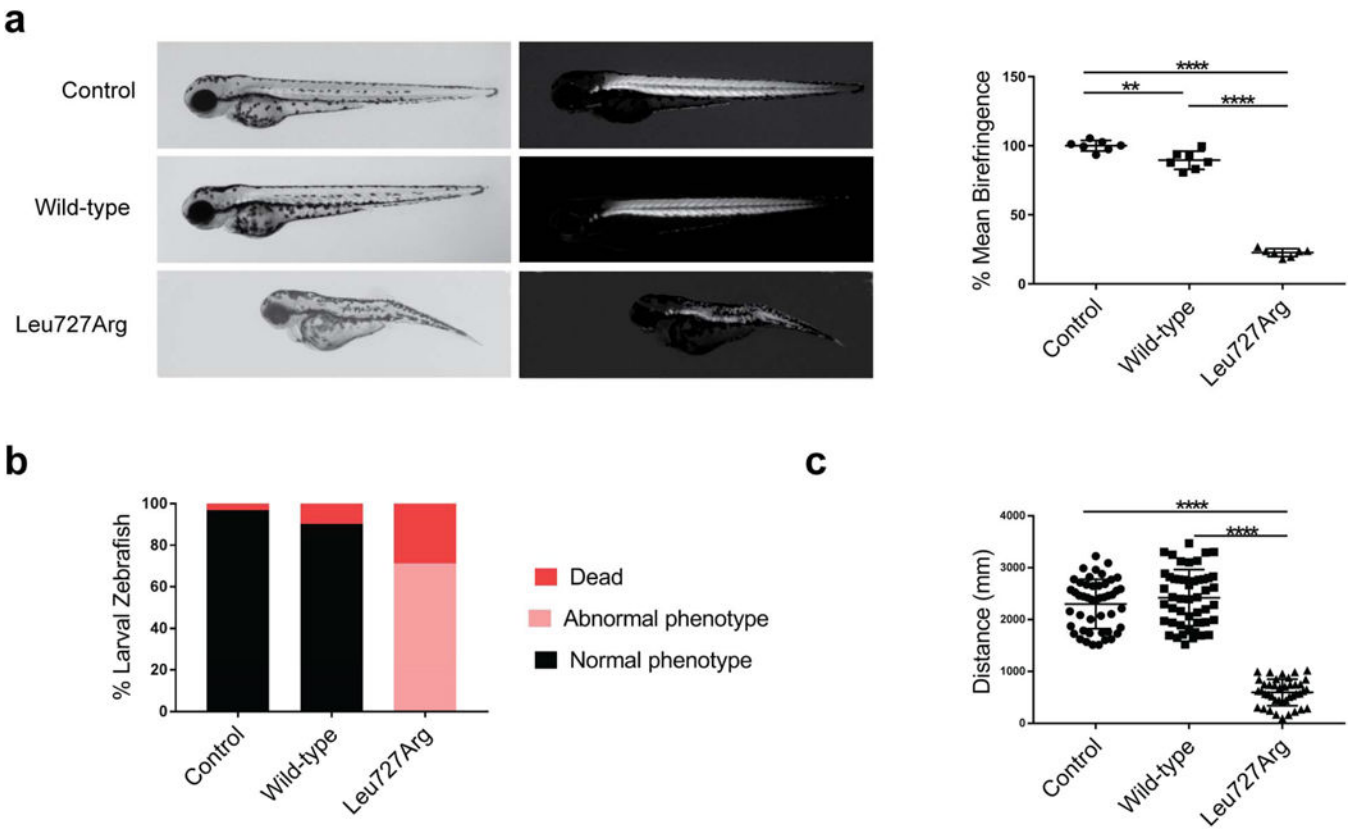

Fig. 6.

Expression of p.Leu727Arg ACTN2 in zebrafish results in functional and morphological defects. **a** Representative zebrafish larvae injected with 100–200 pg of p.Leu727Arg *ACTN2* mRNA exhibit structural muscle defects at 3 dpf. Imaging under polarized light revealed highly reduced birefringence in p.Leu727Arg zebrafish as compared to controls, reflecting an impaired muscle integrity and indicating an abnormal organization of the muscle. **b** Distribution of normal and abnormal (smaller myotome and dorsal curvature) phenotype in zebrafish larvae injected with p.Leu727Arg or wild-type ACTN2 mRNA. **c** Quantification of the distance travelled by p.Leu727Arg or control zebrafish larvae at 3 dpf. The plots display the individual values obtained for each animal, their mean and standard deviation. Normal distribution of the data was assessed with the Shapiro-Wilk normality test. Groups were compared using either one-way ANOVA followed by Bonferroni's post-hoc comparison test (a) or using non parametric tests (c) (Kruskal-Wallis followed by Dunn's post hoc test). **p< 0.01 ; ****p<0.0001

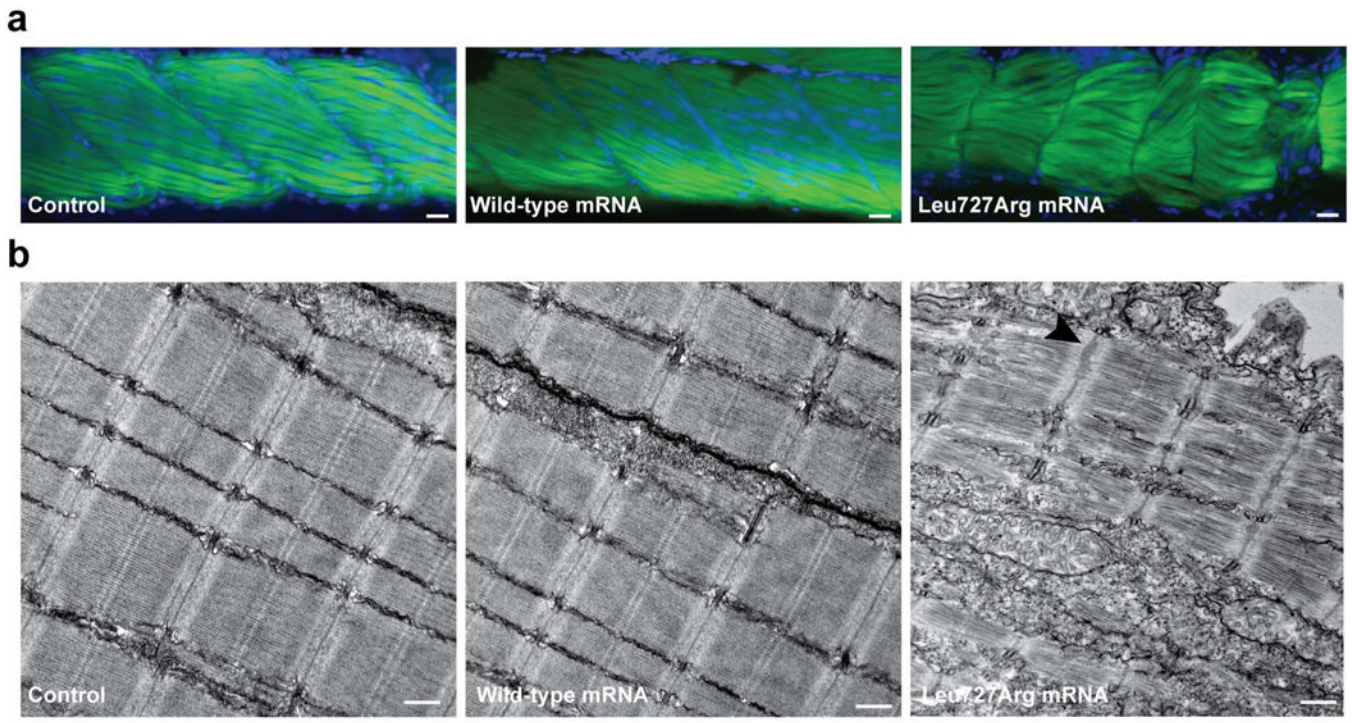

Fig. 7.

Expression of p.Leu727Arg in zebrafish results in skeletal muscle disorganization**. a** Whole-mount phalloidin staining demonstrates smaller somites with profound spacing between adjacent myofibers in p.Leu727Arg-injected zebrafish larvae (3dpf). Scale bar: 2 μm. **b** Ultrastructural evaluation by transmission electron microscopy at 3 dpf shows extensive sarcomeric disorganization and Z-line jagging (arrowhead) in p.Leu727Arg-injected zebrafish larvae. Scale bar: 500 nm

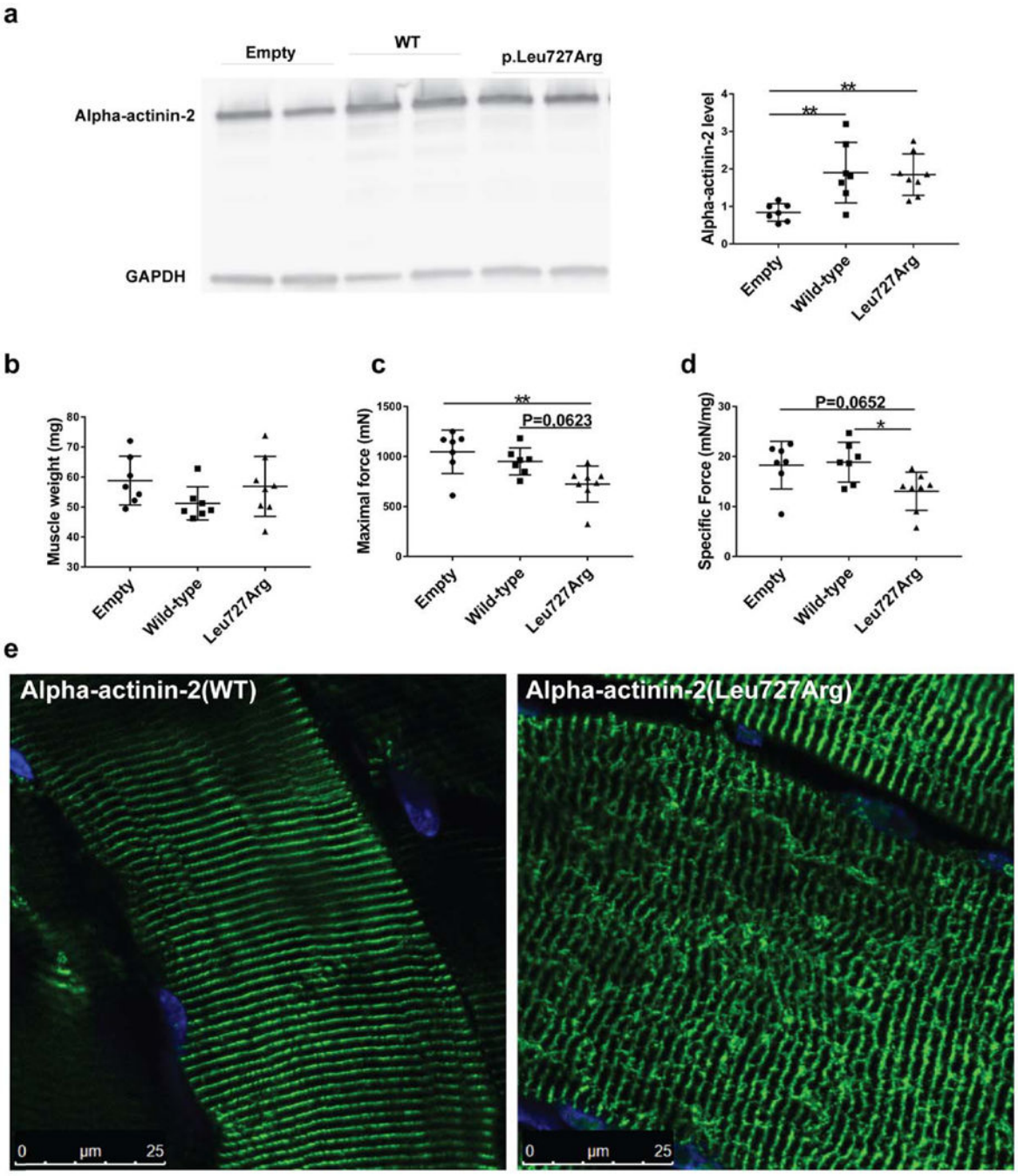

Fig. 8.

Functional and structural defects in mouse tibialis anterior with the p.Leu727Arg ACTN2. **a** SDS-page of tibialis anterior muscle extracts probed with antibodies against alpha-actinin-2 and beta-tubulin. Quantification of alpha-actinin-2 overexpression shows a twofold overexpression in the muscles injected with AAV encoding the wild-type or p.Leu727Arg alpha-actinin-2. **b** Weight of tibialis anterior muscles is similar for all tested conditions. **c** Maximal and **d** specific muscle force of tibialis anterior expressing the p.Leu727Arg mutation is reduced. **e** Longitudinal tibialis anterior muscle sections stained for alpha-

actinin-2 reveals proper localization at the Z-line of both wild-type and mutant proteins but abnormal Z-line organization in the mutant-injected muscle. The plots display the individual values obtained for each animal, their mean and standard deviation. Normal distribution of the data was assessed (Shapiro-Wilk normality test). Groups were compared using either one-way ANOVA followed by Bonferroni's post-hoc comparison test (a, c, d) or using non parametric tests (b) (Kruskal-Wallis followed by Dunn's post hoc test). * $p<0.05$; ** $p< 0.01$

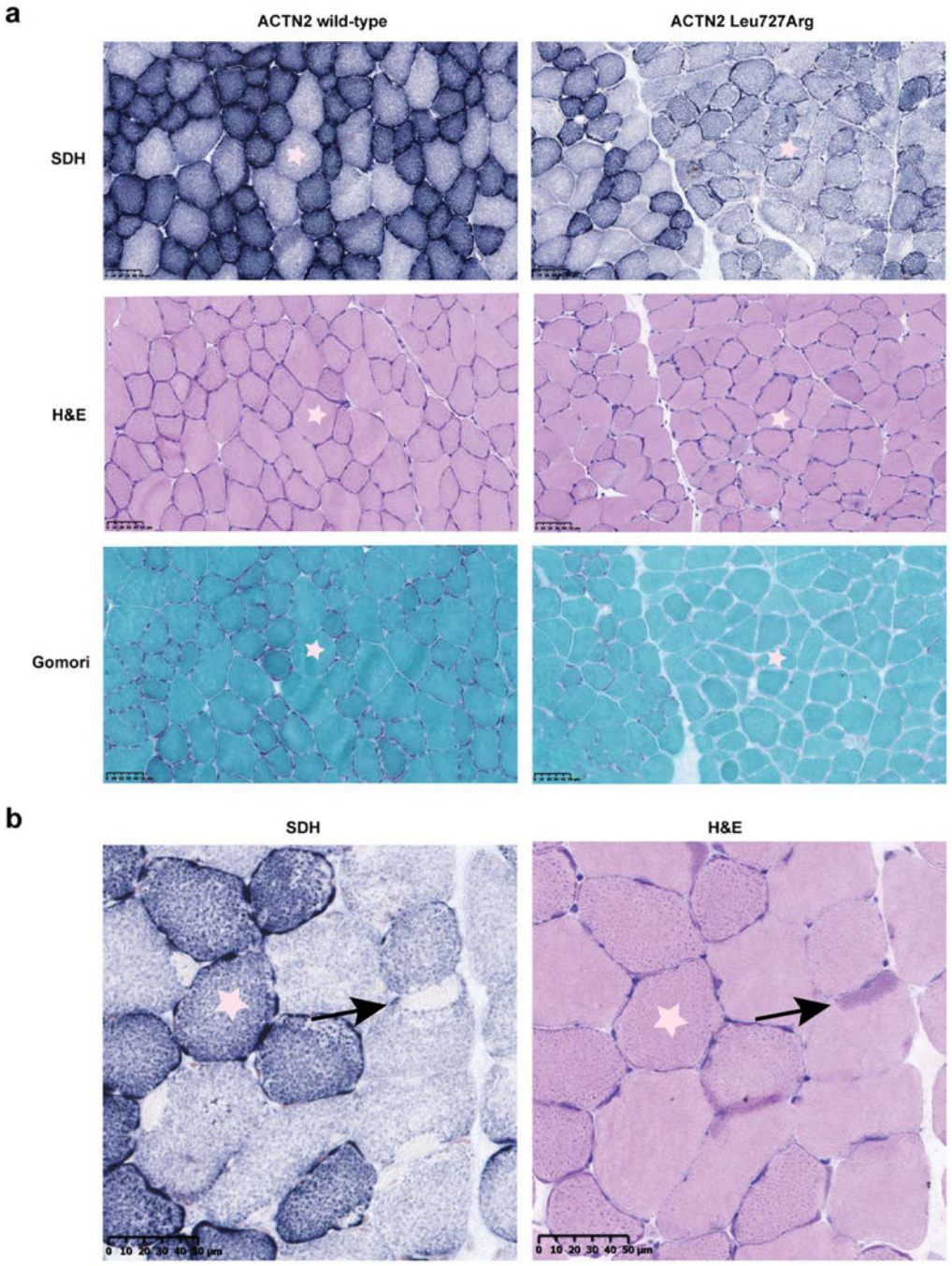

Fig. 9.

Characterization of histological features in mouse tibialis anterior muscles. **a** Transversal sections (serial sections) showing large disorganized regions (SDH) in muscle expressing the p.Leu727Arg mutation. **b** Transversal sections (serial sections) of the muscles expressing the p.Leu727Arg mutation. Some cores revealed with SDH staining are stained darker with H&E (arrows). The stars show corresponding fibers in the different panels

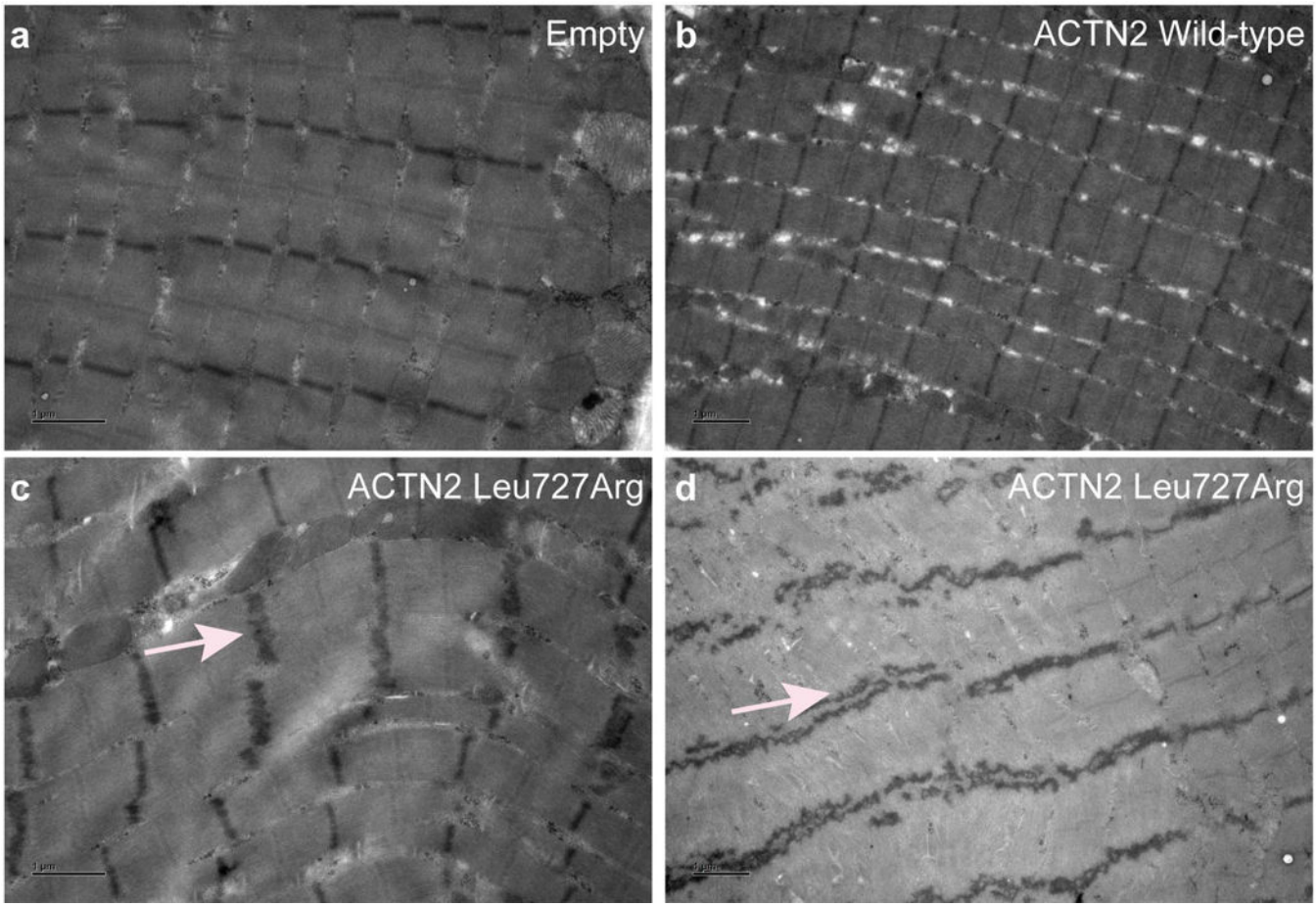

Fig. 10.

Muscle ultrastructural defects caused by mutated *ACTN2* overexpression in mice. Longitudinal sections from tibialis anterior muscles from injected mice. **a** Control mouse muscle injected with empty AAV. **b** Ultrastructure of muscle overexpressing alpha-actinin-2 wild-type is similar to control muscles. **c** Zigzagging appearance of the Z-lines in muscles overexpressing the p.Leu727Arg ACTN2 mutation (arrow). **d** Split Z-line in muscle overexpressing the mutation (arrow)